Phase-space computation of multi-arrival traveltimes, Part I: Theory and concepts

Vladimir Bashkardin[1], *Thomas J. Browaeys*[2], *Sergey Fomel*[1], *Fuchun Gao*[3], *Roman Kazinnik*[4], *Scott A. Morton*[5], *Sergey Terentyev*[5], *Alexander Vladimirsky*[6], *and Paul Williamson*[3]

SUMMARY

In complicated geologic environments with multipathing in traveltime fields, Kirchhoff migration can improve imaging results, if the integration is performed in the angle domain. Angle-domain migration operates on a traveltime table expressed as a function of image points and subsurface angles. For the necessary function to be computed, ray tracing can simply be performed from subsurface locations using different initial take-off angles. Unfortunately, the computational cost of such a bottom-up approach may be prohibitive. However, initial-value ray tracing can be reformulated as escape equations in phase space, which allow for a grid-based solution at a possibly lower cost. In this paper, we derive escape equations for general 2-D and 3-D anisotropic media, derive the reduced phase-space formulation of escape equations, introduce a stable upwind finite-difference discretization, and suggest the use of a hybrid Eulerian-Lagrangian approach for a practical and accurate numerical solution.

INTRODUCTION

Integral-operator Kirchhoff migration remains a staple in the toolbox of imaging practitioners, even in complex geologic settings (Leveille et al., 2011). Fundamentally, this type of imaging rests on a high-frequency approximation of wave propagation and a necessity to compute Green's functions. Various efficient algorithms have been developed over the years for this purpose, all of which generally can be divided into two groups: Eulerian and Lagrangian methods (Engquist and Runborg, 2003; Runborg, 2007).

Finite-difference eikonal solvers belong to the first group. Although they enable a fast computation of minimum-time arrivals between two points (van Trier and Symes, 1991; Sethian and Popovici, 1999; Popovici and Sethian, 2002; Zhao, 2005; Fomel et al., 2009), they are not always sufficient for imaging difficult geologic areas (Geoltrain and Brac, 1993). A frequently used alternative, initial-value ray tracing (Virieux and Farra, 1991; Farra, 1993; Vinje et al., 1993; Gibson, 2000), is a Lagrangian method that produces multiple arrivals.

Incorporation of multiple arrivals into Kirchhoff migration is critical to high-quality imaging in complex geologic environments (Operto et al., 2000). This high quality can be achieved if migration is carried out in the angle domain, which naturally unravels multipathing (Xu et al., 2001; Brandsberg-Dahl et al., 2003). Green's functions for angle-domain migration can be computed using initial-value ray tracing from image locations (Koren and Ravve, 2011), which, however, can be costly and limit the feasibility of such an approach.

Initial-value ray tracing can be reformulated in a Eulerian phase-space framework in the form of escape equations (Fomel and Sethian, 2002), which are partial differential equations that replace the evolution of individual ray trajectories with the flow of escape variables in phase space. Such a formulation potentially enables the computation of everything that is necessary for angle-domain imaging less expensively.

In Part I of this paper, we derive a reduced-phase space formulation for the escape equations in both heterogeneous isotropic and anisotropic media and introduce an upwind finite-difference discretization for them. We then analyze the behavior of the escape functions in phase space and devise a hybrid, Eulerian-Lagrangian strategy for computing accurate numerical solutions to the escape equations. Part II (Bashkardin et al., 2012) describes details of our implementation and its application to angle-domain Kirchhoff migration.

THEORY

Escape equations

For general anisotropic media, the eikonal equation takes the form

$$|\mathbf{p}|^2 - S^2(\mathbf{x},\mathbf{n}) = 0\,, \tag{1}$$

where $\mathbf{p}$ is the phase slowness vector, $\mathbf{n} = \frac{\mathbf{p}}{|\mathbf{p}|}$ is the direction of the traveltime gradient, and $S(\mathbf{x},\mathbf{n})$ is the phase slowness.

Using Hamilton's canonical equations, we can find the system of ray-tracing equations (Červený, 2001)

$$\dot{\mathbf{x}} = \mathbf{p} - S(\mathbf{x},\mathbf{n})\,\nabla_{\mathbf{p}} S\,, \tag{2}$$

$$\dot{\mathbf{p}} = S(\mathbf{x},\mathbf{n})\,\nabla_{\mathbf{x}} S\,, \tag{3}$$

where $\dot{\mathbf{f}}$ denotes $\frac{\mathrm{d}\mathbf{f}}{\mathrm{d}\sigma}$ and σ is a parameter changing along the ray.

These equations define the characteristic directions or rays in phase space. In a finite domain, a ray eventually escapes the phase-space domain at location $\widehat{\mathbf{y}}(\mathbf{x},\mathbf{p})$. For every point on the ray, because the escape location remains constant, we can write

$$\begin{gathered}\dot{\widehat{\mathbf{y}}} = \nabla_{\mathbf{x}}\widehat{\mathbf{y}}\,\dot{\mathbf{x}} + \nabla_{\mathbf{p}}\widehat{\mathbf{y}}\,\dot{\mathbf{p}} = \\ \nabla_{\mathbf{x}}\widehat{\mathbf{y}}\,\left(\mathbf{p} - S\nabla_{\mathbf{p}} S\right) + \nabla_{\mathbf{p}}\widehat{\mathbf{y}}\,\left(S\nabla_{\mathbf{x}} S\right) = 0\,.\end{gathered} \tag{4}$$

Escape traveltime decreases along the ray toward the boundary; therefore, from equations 2 and 3 we can derive $\dot{\widehat{T}} = -S^2$ and write a similar expression:

$$\begin{gathered}\dot{\widehat{T}} = \nabla_{\mathbf{x}}\widehat{T}\cdot\dot{\mathbf{x}} + \nabla_{\mathbf{p}}\widehat{T}\cdot\dot{\mathbf{p}} = \\ \left(\mathbf{p} - S\nabla_{\mathbf{p}} S\right)\cdot\nabla_{\mathbf{x}}\widehat{T} + S\nabla_{\mathbf{x}} S\cdot\nabla_{\mathbf{p}}\widehat{T} = -S^2\,.\end{gathered} \tag{5}$$

[1]The University of Texas at Austin
[2]The University of Texas at Austin (now at Total E&P)
[3]Total E&P
[4]The University of Texas at Austin (now at ConocoPhillips)
[5]Hess Corporation
[6]Cornell University

DOI http://dx.doi.org/10.1190/segam2012-1522.1

Equations 4 and 5 are partial differential equations, which define escape time and locations for all arrivals originating from $\mathbf{x}$ with initial phase vector $\mathbf{p}$ (Fomel and Sethian, 2002).

Reduced phase space

For computational purposes, it is beneficial to derive similar equations in the reduced phase space, in which phase dimensions are replaced with angles associated with the phase vector direction (Osher et al., 2002). Reduced phase space has fewer dimensions, because n components of phase slowness vector $\mathbf{p}$ are related by $(n-1)$ angles.

For a 2-D medium, we define the slowness vector as

$$\mathbf{p}\left(p_x,p_z\right)=\left\{-S\sin\theta,-S\cos\theta\right\}\ ,$$

where θ is the angle between the phase vector and the vertical direction. Then, by using the relations

$$\begin{aligned}\frac{\partial}{\partial p_x}&=\frac{\partial\left(\tan^{-1}\frac{p_x}{p_z}\right)}{\partial p_x}\frac{\partial}{\partial\theta}=-\frac{p_z}{p_x^2+p_z^2}\frac{\partial}{\partial\theta}\ ,\\ \frac{\partial}{\partial p_z}&=\frac{\partial\left(\cot^{-1}\frac{p_z}{p_x}\right)}{\partial p_z}\frac{\partial}{\partial\theta}=\frac{p_x}{p_x^2+p_z^2}\frac{\partial}{\partial\theta}\ ,\end{aligned}\tag{6}$$

we can derive from equation 5 the following equation for escape traveltime in reduced phase space

$$\begin{aligned}\left(S\sin\theta-S_\theta\cos\theta\right)\frac{\partial\widehat{T}}{\partial x}+\left(S\cos\theta+S_\theta\sin\theta\right)\frac{\partial\widehat{T}}{\partial z}+\\ \left(S_x\cos\theta-S_z\sin\theta\right)\frac{\partial\widehat{T}}{\partial\theta}=S^2\end{aligned}\tag{7}$$

where S_θ, S_x, and S_z are angular and spatial derivatives of the phase slowness field, respectively. Escape equations for $\widehat{x}$ and $\widehat{z}$ have their right-hand sides equal to zero.

In a 3-D medium, the phase-vector direction is defined by two angles: θ, the angle between $\mathbf{p}$ and the z axis (inclination), and ϕ, the angle between the projection of p onto the $x-y$ plane and the x axis (azimuth). Then, the vector is

$$\mathbf{p}\left(p_x,p_y,p_z\right)=\left\{-S\sin\theta\cos\phi,-S\sin\theta\sin\phi,-S\cos\theta\right\}\ ,$$

and by changing variables from $\mathbf{p}$ to ϕ, θ and using $\phi=\tan^{-1}\left(\frac{p_y}{p_x}\right)$ and $\theta=\tan^{-1}\left(-\frac{\sqrt{p_x^2+p_y^2}}{p_z}\right)$ for $\frac{\partial}{\partial p_x}$, $\frac{\partial}{\partial p_y}$, $\frac{\partial}{\partial p_z}$ in a way similar to that used in equation 6 we can derive the corresponding reduced phase space equation in 3-D as

$$\begin{aligned}\left(S\sin\theta\cos\phi-S_\theta\cos\theta\cos\phi+S_\phi\frac{\sin\phi}{\sin\theta}\right)\frac{\partial\widehat{T}}{\partial x}+\\ \left(S\sin\theta\sin\phi-S_\theta\cos\theta\sin\phi-S_\phi\frac{\cos\phi}{\sin\theta}\right)\frac{\partial\widehat{T}}{\partial y}+\\ \left(S\cos\theta+S_\theta\sin\theta\right)\frac{\partial\widehat{T}}{\partial z}+\\ \left(S_x\cos\theta\cos\phi\ +S_y\cos\theta\sin\phi-S_z\sin\theta\right)\frac{\partial\widehat{T}}{\partial\theta}+\\ \frac{1}{\sin\theta}\left(S_y\cos\phi\ -S_x\sin\phi\right)\frac{\partial\widehat{T}}{\partial\phi}=S^2\end{aligned}\tag{8}$$

where S_θ, S_ϕ, S_x, S_y and S_z are angular and spatial derivatives of phase slowness. In the isotropic case, S does not depend on θ or ϕ, and $S_\theta=S_\phi=0$.

IMPLEMENTATION PRINCIPLES

Upwind finite differences and sweeping

Escape equations can be written as a general advection system:

$$\mathbf{a}\left(\mathbf{x},\theta,\phi\right)\cdot\nabla_{\mathbf{x},\theta,\phi}\,\widehat{x}=b\ ,\tag{9}$$

where $\mathbf{a}\left(\mathbf{x},\theta,\phi\right)$ is the vector field defining the characteristics (rays) in phase space, $\widehat{x}$ is the escape quantity flowing from the boundaries of the domain along the characteristics, and b is the source term, which is nonzero for quantities changing along the ray (e.g., traveltime). The equation itself describes a steady-state solution, but the correct numerical scheme for it must realize a numerical flow of information from appropriate boundary conditions.

Our choice of a numerical technique for solving equation 9 is dictated by the fact that the resulting solver will be eventually used to compute Green's functions for 3-D Kirchhoff migration. This implies that the algorithm should generate output on a structured rectangular grid and scale to five dimensions. These requirements impose application of a finite-difference (F-D) discretization. The above advection system should be discretized in each dimension according to the upwind principle, i.e., the F-D stencil for current point ought to be skewed toward the opposite direction of the flow. The first- and second-order stencils in one dimension are given, respectively, by the following expressions (Hirsch, 2007):

$$\frac{\partial\widehat{x}}{\partial x_k}\approx\begin{cases}\frac{\widehat{x}_i-\widehat{x}_{i-1}}{\Delta x_k}, & a_{k,i}>0\\ \frac{\widehat{x}_{i+1}-\widehat{x}_i}{\Delta x_k}, & a_{k,i}<0\end{cases}\ ,\tag{10}$$

$$\frac{\partial\widehat{x}}{\partial x_k}\approx\begin{cases}\frac{3\widehat{x}_i-4\widehat{x}_{i-1}+\widehat{x}_{i-2}}{2\Delta x_k}, & a_{k,i}>0\\ \frac{-\widehat{x}_{i+2}+4\widehat{x}_{i+1}-3\widehat{x}_i}{2\Delta x_k}, & a_{k,i}<0\end{cases}\ ,\tag{11}$$

where x_k is the k-th axis of the reduced-phase space volume, Δx_k is the grid sampling along the axis, $\widehat{x}_i$ is the escape value at the i-th node of the same dimension, and $a_{k,i}$ is the k-th component of vector $\mathbf{a}\left(\mathbf{x},\theta,\phi\right)$ at the same location.

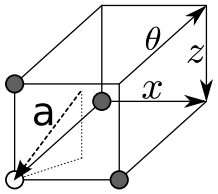

Figure 1: First-order finite-difference stencil in 3-D reduced phase space cell; white point is being computed, whereas gray points are parent points with known values.

After discretization, equation 9 turns into a system of linear equations,

$$\bar{\mathbf{A}}\,\widehat{\mathbf{x}}=\mathbf{b}\ ,\tag{12}$$

where $\bar{\mathbf{A}}$ is a sparse matrix comprising upwind F-D stencil coefficients. This system can be solved iteratively in a number of ways. The Gauss-Seidel method is used frequently, because it allows construction of a new solution from the previous iteration "in place" without generating extra copies of the data. For faster convergence, Gauss-Seidel iterations should incorporate alternating directions akin to those of the fast sweeping method for the eikonal equation (Zhao, 2005). Changing di-

DOI http://dx.doi.org/10.1190/segam2012-1522.1

rections allows the solver to propagate escape values from the boundaries inside the domain in all possible directions.

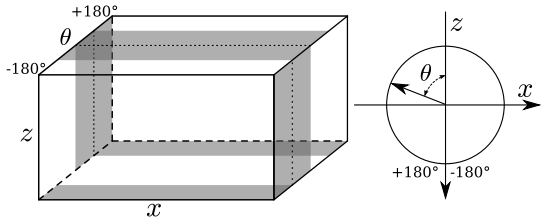

Figure 2: Boundary conditions for escape equations in 3-D reduced phase space with an isotropic slowness model. Domain is periodic in θ direction.

Figure 2 shows rectangular patches (shaded in gray) of points with known escape values ($\widehat{\mathbf{y}} = \mathbf{x}, \widehat{T} = 0$) at the beginning of the computation for an arbitrary isotropic model. It is easy to see that, in the isotropic case, advection vector components a_x and a_z do not change signs for the constant θ; therefore, only alternating directions along the angular axis are needed. However, if the model is anisotropic, sweeping directions should be changed along all axes. Furthermore, boundary conditions in this case might be composed of nonrectangular patches.

Accuracy and a Eulerian-Lagrangian approach

Upwind discretization and Gauss-Seidel sweeping with alternating directions provide a stable numerical scheme but do not guarantee sufficient accuracy. In order to analyze errors in a typical solution, we tested simple F-D implementations on the Marmousi model (Versteeg (1993),Figure 3(a)) using fine spatial sampling Δx=Δz=4 m and angular sampling $\Delta\theta$=1°.

Figures 3(b), 3(c) and 3(d) show escape quantities $\widehat{T}$, $\widehat{z}$, and $\widehat{x}$ computed using ray tracing for all locations and angles at the z=2 km slice in reduced phase space. Each location at these plots is color coded according to the exit location and time for the ray that originated from it. All escape solutions clearly exhibit areas of smoothly changing values and regions of rapidly changing values – the latter is a well-known effect in initial-value ray tracing, when a small change in initial conditions causes a large change in the solution. Application of F-D stencils in such places produces dissipation and/or dispersion, depending on their order. Figures 3(e) and 3(f) demonstrate extracted slices for the same depth from a phase-space solution for $\widehat{x}$ with first- and second-order F-D solvers, respectively. Both solvers are clearly incapable of preserving details of the solution in difficult places. The second-order F-D produces less dissipation, but the error remains noticeable. Moreover, numerical dissipation in high-gradient regions propagates into smoother subareas and makes the whole solution unreliable for later imaging because arrivals either get destroyed (do not exit on the surface) or exit in incorrect places.

Another source of numerical errors is related to the footprint of the domain corners, which shows up regardless of the complexity of the slowness model. Because of the rectangular shape of the domain, escape solutions are not differentiable along lines emanating from the domain corners. Both F-D stencils produce noticeable errors when applied to these regions.

A usual remedy for the first problem in the Eulerian framework would be adaptive mesh refinement (Plewa et al., 2005) and/or application of an F-D stencil of a higher order. However, these methods may be computationally impractical in 5-D phase space. In addition, the effectiveness of higher-order, accurate discretizations is limited by the second problem, which is related to the nonsmoothness of boundary conditions for escape variables.

A different strategy that allows the inhibition of numerical dissipation in advection problems is to use accurate Lagrangian solutions at grid points where desired accuracy can not be acquired with F-D stencils. Such hybrid, Eulerian-Lagrangian schemes often enable remarkable improvement in accuracy without costly grid refinement (Ferziger and Perić, 2002). Before applying the F-D stencil to a group of upwind points, we check if the Euclidean distances between their escape locations are smaller than some predefined threshold. If this value is exceeded, the ray tracing is computed for the current location in the grid. Newly obtained escape values are then locked in for future sweeping iterations.

Our tests indicate that, even in the most complicated models, only a small fraction of points will be computed with ray tracing so as to achieve accuracy similar to that of the fully traced escape solution (see Figure 3(d)). The vast majority of points can still be computed with upwind finite differences.

Compared to the full Lagrangian (ray tracing) solution of the same resolution, the cost is reduced from $O\left(N_{\mathbf{x}} N_{\mathbf{a}} N_{\mathbf{x}}^{1/D}\right)$ to $O\left(N_{\mathbf{x}} N_{\mathbf{a}} N_{\mathrm{GS}}\right)$, where $N_{\mathbf{x}}$ is the number of subsurface locations, $N_{\mathbf{a}}$ is the number of angular directions, $N_{\mathbf{x}}^{1/D}$ is the cost of ray tracing (D is the dimensionality of the spatial domain $\mathbf{x}$), N_{GS} is the number of Gauss-Seidel iterations.

CONCLUSIONS

We have derived escape equations in reduced phase space for general 2-D and 3-D anisotropic media and formulated general principles for implementation of a stable and accurate algorithm for computing multi-arrival traveltimes on a phase-space grid. The proposed approach employs a hybrid Eulerian-Lagrangian strategy and requires us to perform ray tracing only for a small fraction of points inside the phase space volume.

Part II of this paper (Bashkardin et al., 2012) addresses the challenges of scalability of the proposed method in 3-D, introduces the concept of a narrow band that enables application of our escape solver to large-scale problems, and demonstrates its use for Kirchhoff imaging in the angle domain.

ACKNOWLEDGMENTS

We thank Hess and Total for supporting this work and for permission to publish the results.

DOI http://dx.doi.org/10.1190/segam2012-1522.1

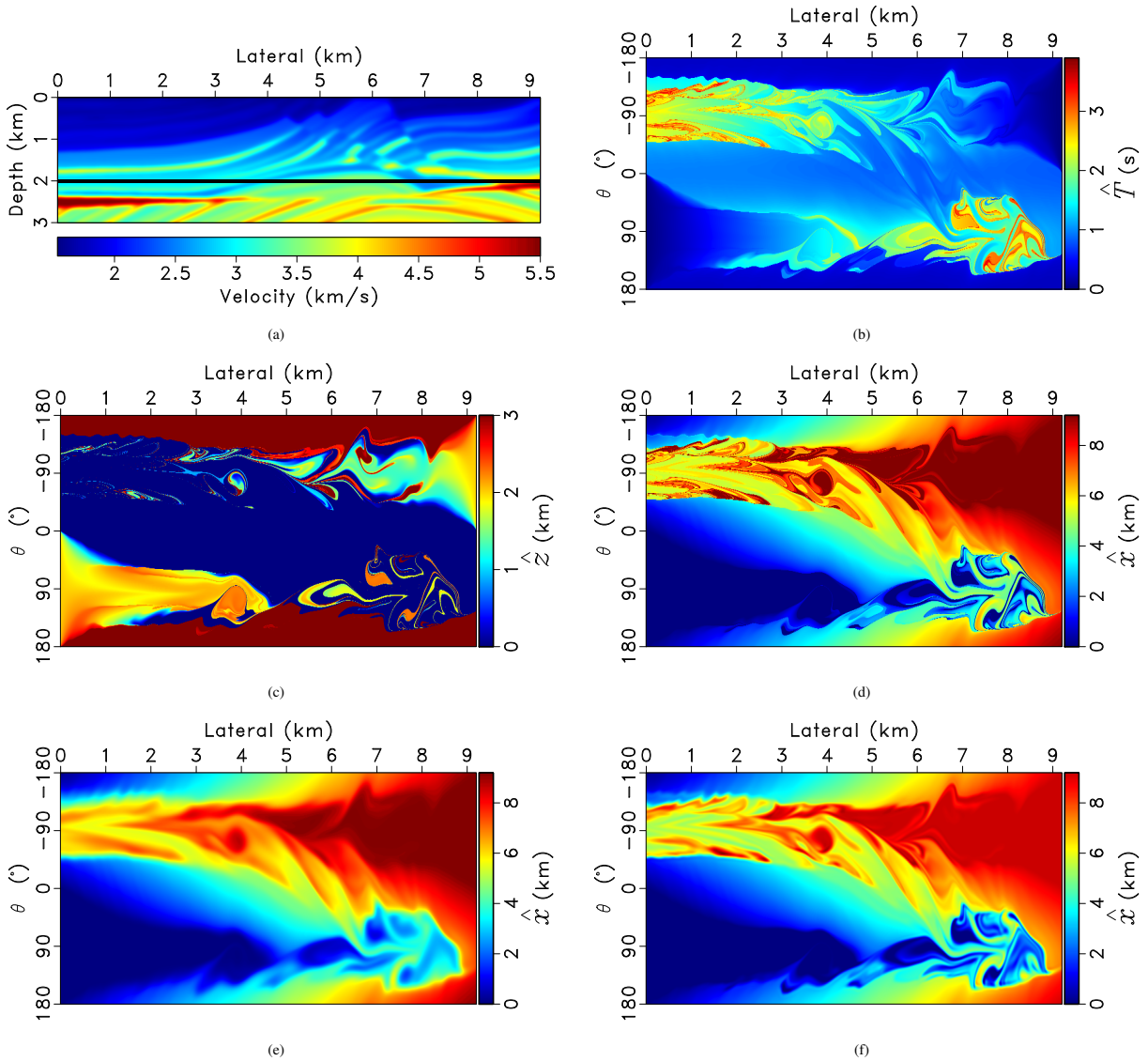

Figure 3: Escape traveltime (b), escape depth (c), escape position (d) computed with ray tracing at z=2 km for Marmuousi model (a); slices for same depth extracted from finite-difference solutions with first-order stencil (e) and second-order stencil (f).

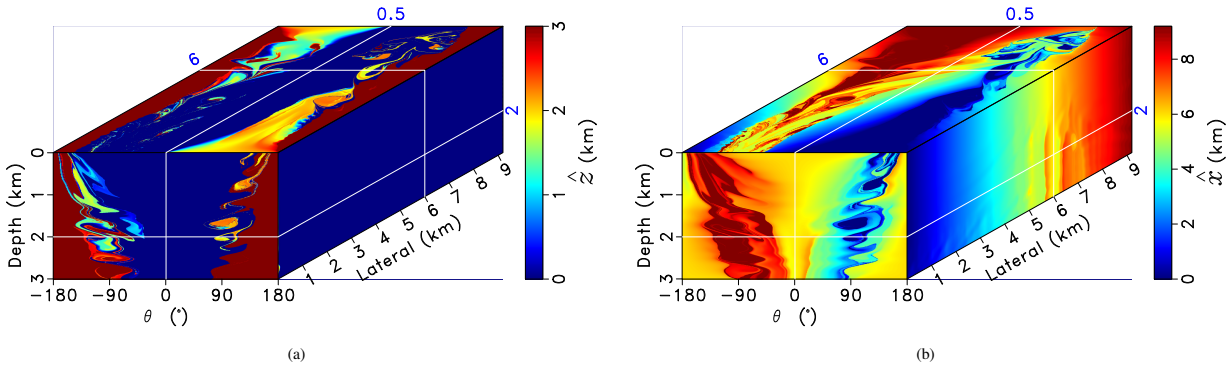

Figure 4: Escape volumes for Marmousi model: depth (a), position (b).

DOI http://dx.doi.org/10.1190/segam2012-1522.1

http://dx.doi.org/10.1190/segam2012-1522.1

EDITED REFERENCES

Note: This reference list is a copy-edited version of the reference list submitted by the author. Reference lists for the 2012 SEG Technical Program Expanded Abstracts have been copy edited so that references provided with the online metadata for each paper will achieve a high degree of linking to cited sources that appear on the Web.

REFERENCES

Bashkardin, V., T. J. Browaeys, S. Fomel, F. Gao, S. A. Morton, S. Terentyev, and A. Vladimirsky, 2012, Phase-space computation of multi-arrival traveltimes: Part II — Implementation and application to angle-domain imaging: Presented at the 82nd Annual International Meeting, SEG.

Brandsberg-Dahl, S., M. V. de Hoop, and B. Ursin, 2003, Focusing in dip and AVA compensation on scattering angle/azimuth common image gathers: Geophysics, **68**, 232–254.

Cerveny, V., 2001, Seismic ray theory: Cambridge University Press.

Engquist, B., and O. Runborg, 2003, Computational high frequency wave propagation: Acta Numerica, **12**, 181–266.

Farra, V., 1993, Ray tracing in complex media: Journal of Applied Geophysics, **30**, 55–73.

Ferziger, J. H., and M. Peric, 2002, Computational methods for fluid dynamics: Springer.

Fomel, S., S. Luo, and H. Zhao, 2009, Fast sweeping method for the factored Eikonal equation: Journal of Computational Physics, **228**, 6440–6455.

Fomel, S., and J. A. Sethian, 2002, Fast-phase space computation of multiple arrivals: Proceedings of the National Academy of Sciences of the United States of America, **99**, 7329–7334.

Geoltrain, S., and J. Brac, 1993, Can we image complex structures with first-arrival traveltime?: Geophysics, **58**, 564–575.

Gibson, R. L., 2000, Ray tracing by wavefront construction for anisotropic media: 70th Annual International Meeting, SEG, Expanded Abstracts, **19**, 2305–2308.

Hirsch, C., 2007, Numerical computation of internal and external flows: Fundamentals of computational fluid dynamics: Elsevier/Butterworth-Heinemann.

Koren, Z., and I. Ravve, 2011, Full-azimuth subsurface angle domain wavefield decomposition and imaging Part I: Directional and reflection image gathers: Geophysics, **76**, no. 1, S1–S13.

Leveille, J. P., I. F. Jones, Z.-Z. Zhou, B. Wang, and F. Liu, 2011, Subsalt imaging for exploration, production, and development: A review: Geophysics, **76**, no. 5, WB3–WB20.

Operto, M. S., S. Xu, and G. Lambare, 2000, Can we quantitatively image complex structures with rays?: Geophysics, **65**, 1223–1238.

Osher, S., L.-T. Cheng, M. Kang, H. Shim, and Y.-H. Tsai, 2002, Geometric optics in a phase-space-based level set and Eulerian framework: Journal of Computational Physics, **179**, 622–648.

Plewa, T., T. J. Linde, and V. G. Weirs, 2005, Adaptive mesh refinement — Theory and applications: Springer.

Popovici, A. M., and J. A. Sethian, 2002, 3D imaging using higher order fast marching traveltimes: Geophysics, **67**, 604–609.

Runborg, O., 2007, Computational high-frequency wave propagation: Communications in Computational Physics, **2**, 827–880.

Sethian, J. A., and A. M. Popovici, 1999, 3D traveltime computation using the fast-marching method: Geophysics, **64**, 516–523.

van Trier, J., and W. W. Symes, 1991, Upwind finite-difference calculation of traveltimes: Geophysics, **56**, 812–821.

Versteeg, R. J., 1993, Sensitivity of prestack depth migration to the velocity model: Geophysics, **58**, 873–882.

Vinje, V., E. Iversen, and H. Gjøystdal, 1993, Traveltime and amplitude estimation using wavefront construction: Geophysics, **58**, 1157–1166.

Virieux, J., and V. Farra, 1991, Ray tracing in 3D complex isotropic media: An analysis of the problem: Geophysics, **56**, 2057–2069.

Xu, S., H. Chauris, G. Lambare, and M. Noble, 2001, Common-angle migration: A strategy for imaging complex media: Geophysics, **66**, 1877–1894.

Zhao, H.-K., 2005, A fast sweeping method for Eikonal equations: Mathematics of Computation, **74**, 603–627.